JOURNAL OF GEOPHYSICAL RESEARCH, VOL. 93, NO. C6, PAGES 6789–6798, JUNE 15, 1988

# Time Evolution of Surface Chlorophyll Patterns From Cross-Spectrum Analysis of Satellite Color Images

KENNETH L. DENMAN

*Department of Fisheries and Oceans, Institute of Ocean Sciences, Sidney, British Columbia, Canada*

MARK R. ABBOTT[1]

*Scripps Institution of Oceanography, University of California, San Diego, La Jolla*
*Jet Propulsion Laboratory, California Institute of Technology, Pasadena*

Sequences of coastal zone color scanner (CZCS) images from the offshore region adjacent to Vancouver Island, Canada, have been analyzed to estimate the time rate of decorrelation of surface phytoplankton chlorophyll pigment patterns. In these high-latitude, high-pigment areas, CZCS-derived pigment estimates were lower than those obtained from ship samples by about a factor of 3, their frequency distributions were skewed in opposite directions, and subareas of the images often showed a discontinuity in the frequency distribution at a concentration of 1.5 mg $m^{-3}$, where the algorithm changes CZCS bands. We selected cloud-free subareas that were common to several images separated in time by 1–17 days. Image pairs were subjected to two-dimensional auto spectrum and cross-spectrum analysis in an array processor, and spectra of squared coherence were formed. The squared coherence estimates for several wave bands were plotted against time separation, in analogy with a time-lagged cross correlation function. Threshold levels for significant coherence were estimated from many realizations of squared coherence calculated for pairs of synthetic random uncorrelated fields with specified power law behavior $\kappa^{-1.5}$, near the observed range $\kappa^{-1.5}$–$\kappa^{-2}$. For wavelengths of 50–150 km, significant coherence is lost after 7–10 days, and for wavelengths of 25–50 km, significant coherence is lost after 5–7 days; in both cases offshore regions maintain coherence longer than coastal regions. For wavelengths of 12.5–25 km, only the offshore regions maintained coherence after 1 day, but that was clearly lost after the next time separation of 6 days. The implication for the formation of monthly average large-scale surface maps to estimate open ocean productivity (e.g., Esaias et al., 1986) is that all mesoscale patterns (< 150-km length scale) will not be resolved.

## INTRODUCTION

The wide variety of time and space scales at which physical and biological processes occur in the ocean is both a source of fascination and a property of fundamental scientific importance [e.g., *Stommel*, 1963; *Haury et al.*, 1978]. It can also be a source of frustration in the design of a program of observations to resolve certain processes unambiguously or to search for causal correlations between physical and biological events [e.g., *Denman and Powell*, 1984]. Moored instruments provide high resolution in time but limited spatial coverage. Drifting instruments provide a Lagrangian time series following but a single parcel of water. Ship surveys can cover a limited area and are not synoptic, and vertical resolution must usually be traded off against horizontal resolution (a grid of stations or continuous underway sampling).

Satellite imagery has promised (and in most cases provided) information on the ocean over a range of scales not attainable previously [e.g., *Brown and Cheney*, 1983; *Maul*, 1985; *Robinson*, 1985; *Stewart*, 1985]. We have learned much about joint physical and biological processes in the ocean from satellite measurements of sea surface temperature [e.g., *Njoku et al.*, 1985] and of phytoplankton plant pigment derived from the coastal zone color scanner (CZCS) on Nimbus 7 [e.g., *Gordon et al.*, 1983*a*]. However, despite the capability of satellites to provide a synoptic two-dimensional sampling of the ocean over a spatial range of 3 decades (1–$10^3$ km), quantitative and statistical approaches to image analysis of the variability of mesoscale patterns in plant pigment and sea surface temperature have been underutilized.

The description and explanation of spatial patterns in plankton communities is a topic of intense interest to biological oceanographers [e.g., *Steele*, 1978]. Current plans to estimate global patterns of primary production by phytoplankton from satellite [*National Academy of Sciences*, 1984; *Brewer et al.*, 1986] require composite scenes formed from cloud-free areas of all available images for the desired time period [*Esaias et al.*, 1986]. Some work has been done on temporal rates of decorrelation of mesoscale patterns to determine the maximum time period over which composite maps are meaningful. In an energetic coastal regime off northern California, *Kelly* [1983, 1985] obtained an estimate of decorrelation time for sea surface temperature patterns in satellite images of 4–5 days, by calculating the time separation at which the structure function (mean square difference between images of temperature averaged over 5 km by 5 km boxes) begins to flatten out. For ship surveys of a coastal area off Vancouver Island, Canada, *Denman and Freeland* [1985] found that variance associated with the temporal structure function at all lags of less than 10 days of temperature and salinity, averaged over the top 10 m, was 0.54 and 0.07 of the average spatial survey variance (maximum dimension of ~100 km). The temporal variance within the time taken for a typical ship survey was then at most half the spatial variance over the survey area, thus ensuring that the spatial maps formed from the survey data made sense. Similarly, *Kosro* [1987] determined a tempo-

[1]Now at College of Oceanography, Oregon State University, Corvallis.



Paper number 8C0235.
0148-0227/88/008C-0235$05.00

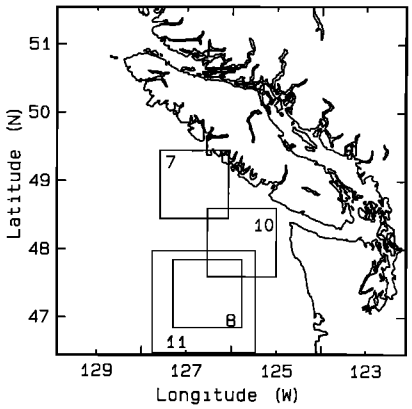


Fig. 1. Map showing the area around Vancouver Island, Canada, included in the coastal zone color scanner images. The square boxes numbered 7, 8, 10, and 11 are the subareas on which cross-spectrum analysis was performed. Subarea 10 is from 1980; the others are from 1981.

ral decorrelation time scale of about 5 days from the first four empirical orthogonal functions of spatial surveys of near-surface currents of a coastal area off northern California, obtained by shipboard Doppler acoustic log.

None of these studies give information on the decorrelation time as a function of spatial scale. In the case of analysis of satellite imagery, these times are required to determine what is the smallest spatial pattern that can be preserved after, say, weekly or monthly averaging to form the composite pigment maps presented by *Esaias et al.* [1986]. In the case of ship surveys, these times are required to design appropriate sampling grids constraining the largest and smallest scales that can be sampled in a given time. The dependence of decorrelation time on spatial scale would be expected to change between different coastal and offshore regimes.

The object of this paper is to estimate from sequences of CZCS images the rate of decorrelation of surface pigment patterns as a function of the time separation between pairs of images. An obvious tool would seem to be the lagged cross-correlation function between images $r^2(0, \tau)$, with spatial lag of zero and time lag $\tau$, but such a correlation will be dominated by large-scale trends. For each pair of images with time separation $\tau$, we will calculate a scale-dependent analog of $r^2$, namely the squared coherence $K_{12}{}^2(\kappa)$ which is a function of scalar inverse wavelength $\kappa$. (In this paper we will refer to $\kappa$ loosely as a "wave number," although $\kappa$ will be smaller than a true wave number by the factor $2\pi$.) Two-dimensional autospectra and cross spectra formed from each pair of images will be summed azimuthally over rings of radius $\kappa = (k^2 + l^2)^{1/2}$ and thickness $\Delta\kappa$, eventually to form the equivalent one-dimensional squared coherence spectrum $K_{12}{}^2(\kappa)$. For each wave band $\kappa$, the squared coherences will be plotted against time separation $\tau$, in analogy with $r^2(0, \tau)$. The rate of decrease with increasing time separation of squared coherence for a given wave band $\kappa$ will represent the rate of pattern decorrelation at the length scale $\kappa^{-1}$.

## METHODOLOGY

### *Processing of CZCS Color Imagery to Pigment Values*

The study area is the Pacific Ocean adjacent to Vancouver Island, Canada (Figure 1), chosen because of extensive multidisciplinary observational work in the region since 1978, when the CZCS was first launched. The CZCS imagery was collected at the Scripps Satellite Oceanography Facility, La Jolla, California, and processed at the Jet Propulsion Laboratory (JPL), Pasadena, California, with software developed by O. Brown and R. Evans (University of Miami, Miami, Florida). Briefly, raw data were corrected for inaccuracies in time, roll, pitch, yaw, and tilt angle of the moveable mirror. A 1024 × 1024 pixel area was selected out of each satellite pass, with a center at 49°N, 126°W, just west of Vancouver Island. These areas were remapped to an equirectangular grid of 512 × 512 pixels where each pixel is 1.1 km on a side (1′ of latitude). For simplicity we use the approximation that a pixel is 1 km on a side.

Atmospheric corrections were made and near-surface concentration of phytoplankton pigment was estimated from the CZCS processing procedures described by *Gordon et al.* [1983*a*, *b*] and *Zion* [1983]. These algorithms yield pigment values with accuracy (compared with field calibration samples) of $\pm 0.3$ log ⟨pigment⟩, but most field comparisons have been for pigment concentrations of less than 1 mg $m^{-3}$ and at latitudes of less than 35°. However, for 11 ship samples in the Coastal Ocean Dynamics Experiment (CODE) area off northern California with in situ chlorophyll ranging from 0.1 to 11.0 mg $m^{-3}$, *Abbott and Zion* [1987] did obtain agreement with satellite-derived chlorophyll ($r^2 = 0.8$ and slope = 1.0, for both variables on linear scales), and for 44 samples off the western English Channel ranging from 0.5 to 50 mg $m^{-3}$, *Holligan et al.* [1983*a*] obtained similar agreement ($r^2 = 0.82$ and standard deviation of estimation of log chlorophyll = 0.26).

In this paper we will present comparisons from latitudes of greater than 48° of satellite-derived estimates of chlorophyll concentrations with ship-sampled calibration values in excess of 30 mg $m^{-3}$. The CZCS algorithms we have used may be inaccurate in regions of high pigment concentration where the water-leaving radiance at 670 nm is nonzero. An iterative approach such as that suggested by *Smith and Wilson* [1981] may be more appropriate. However, because few of the required optical measurements [e.g., *Austin and Petzold*, 1981] have been made at these high pigment concentrations, this approach cannot easily be extended to the coastal waters off Vancouver Island.

### *Algorithms for Spectrum Analysis*

Statistical and spectrum analyses of the 512 by 512 pixel images of pigment concentrations were performed at the Institute of Ocean Sciences and at Interact Research and Development Corporation, both in Sidney, British Columbia, Canada, with software developed by A. Dolling (Interact). First, a 3 × 3 running median filter is applied to all images to remove noise spikes or dropout, and out of range values resulting from cloud and land are set to zero.

The images contain much of Vancouver Island and usually a large fraction of cloud. We search the images for clear oceanic subareas that are common to several images obtained within a 2-week period or less. Because we wish to operate on the whole 512 × 512 image in an array processor, all values outside a selected (square $n \times n$) subarea are set to zero (boxcar filter), and the mean within the subarea is calculated and subtracted from the field within the subarea. Four subareas for which the results are presented here are shown in Figure 1. Since the spectral transform is applied to the whole image of Figure 1, we apply a cosine taper to the residuals, with a 10% taper at each end of the subarea, first in the

east-west direction and then in the north-south direction. Otherwise, the edges of the subarea cause (sometimes) severe ringing within the calculated autospectrum.

To obtain autospectra, a two-dimensional fast Fourier transform (FFT) is performed on each image in the array processor. Equivalent one-dimensional autospectra are formed by azimuthal summation within circular rings of constant radial magnitude $\kappa$. Ring widths $\Delta\kappa$ can be constant, or they can increase geometrically (width constant on a log plot) to remove high-wave number jitter. All estimates outside the largest ring were summed into a single highest $\kappa$ estimate. Because the spectral estimates are formed by summing rather than smoothing, there is no leakage across wave numbers, and the total variance of the image in $(x, y)$ space (after boxcar filter, mean removal, and cosine taper) equals the sum of the spectral estimates. Because the whole $512 \times 512$ image is transformed in the array processor, spectral estimates for $\kappa < 1/n$ (in reciprocal kilometers) are meaningless and are set to zero.

The complex cross spectrum between two images, $s_{12}(\kappa)$, is also formed by two-dimensional FFT: $s_{12}(\kappa) = c_{12}(\kappa) - iq_{12}(\kappa)$, where $c_{12}$ and $q_{12}$ denote the cospectrum and the quadrature spectrum. They are first summed azimuthally to give one-dimensional cospectrum $C_{12}(\kappa)$ and quadrature spectrum, $Q_{12}(\kappa)$, and then the one dimensional squared-coherence estimate is formed:

$$K_{12}^2(\kappa) = \frac{C_{12}^2(\kappa) + Q_{12}^2(\kappa)}{S_{11}(\kappa)S_{22}(\kappa)}$$

The squared coherence estimate $K_{12}^2(\kappa)$ between two images is the analog for a given wave number $\kappa$ of the squared cross-correlation coefficient between two images formed from the variance and covariance estimates $v_{ij}(\tau)$, all taken at zero spatial lag:

$$r_{12}^2(0) = \frac{v_{12}^2(\tau)}{v_{11}(0)v_{22}(0)}$$

The cross-correlation coefficient $r$ represents the correlation between two images over the whole subarea and is usually heavily dependent on correlation at the largest scales within the subarea. Finally, we plot $K^2$ for different bands of $\Delta\kappa$ against $\tau$, the time separation between the image pairs, thereby obtaining an estimate of the temporal rate at which surface patterns of chlorophyll pigment evolve and decorrelate. At smaller scales (larger $\kappa$), the patterns should decorrelate faster.

### *Diagnostic Calculations and Significance Levels*

We performed several diagnostic calculations in an effort to avoid spurious features in the spectra caused by the analyses. First, we formed synthetic spectra with power law behaviors of $\kappa^0$, $\kappa^{-1}$, and $\kappa^{-2}$ by randomizing the complex spectral amplitudes as bivariate Gaussian variables (by the Box-Muller technique). The spectra were then inverse transformed to form synthetic images with the prescribed spectral behavior. The FFT was then performed on images with and without the addition of spatially uncorrelated white noise, and the spectra were compared with the original spectrum. We also tested the effects individually and sequentially of the $3 \times 3$ running median, the boxcar filter, and the cosine taper on the resulting spectra. In general, the effects were as expected: the $3 \times 3$ median filter removed noise at high wave numbers, the boxcar filter caused strong ringing if the mean within the subarea was not removed, and the cosine taper effectively removed this ringing at wave numbers above about 0.1 $km^{-1}$. (The maximum $\kappa$ for the remapped image was the Nyquist value $(2 \times 1.1\ km)^{-1}$, although pixel spacing in the original image could be as large as 2.5 km near the edge of a scan at full forward tilt.) We later tested the effect of removal of an $(x, y)$ plane from the data within the subarea, for several real images. The differences between the calculated spectra with and without $(x, y)$ plane removal were not significant, presumably because of the cosine tapering.

Spectral estimates of squared coherence between two series can be assigned confidence limits, or they can be tested for nonzero significance (at some significance level) relative to expected coherence between two random uncorrelated series. We doubted the relevance of such significance levels to two-dimensional data, especially after operation by the boxcar filter to produce a nonzero subarea within the larger image (mostly zeroes) on which the spectral transformation was carried out. Thus we calculated the squared coherence spectrum between many pairs of synthetic random uncorrelated images with the appropriate spectral shape for the various bandwidths $\Delta\kappa$ that we used. In most cases, out of 99 realizations we chose the tenth highest estimate at each $\kappa$ as an estimate of the 90% significance level for squared coherence. That is, only 1 out of 10 estimates of squared coherence between two random uncorrelated images would be expected to exceed this value. For the most common subarea and bandwidth combination, we performed 999 realizations and took the one hundredth highest in each wave number band as the 90% significance level. In general, the latter estimates were a smoother function of $\kappa$ than those based on 99 realizations because the tail of the distribution was sampled more adequately.

We formed frequency distribution histograms and calculated basic statistics for the images as stored in log-transformed format. Because phytoplankton tend to be logarithmically distributed in nature (i.e., distributions of log-transformed variates tend to be more nearly Gaussian normal (for example, *Smith and Baker* [1982] and this work)), we calculated the autospectrum for a clear $200 \times 200$ pixel subarea of real image both on the original log-transformed values and on converted derived chlorophyll values. As the final autospectra did not differ significantly, we henceforth computed all autospectra and cross spectra on the linear chlorophyll values.

## RESULTS

### *Sequences of Images*

We searched several years' data and identified two sequences of images with common clear subareas within the scene shown in Figure 1. The sequences consist of five images in July–August 1980 with one subarea (10) and three images in September 1981 with three subareas (7, 8, and 11), all shown in Figure 1. Subarea 11 encloses 8, but we thought a comparison of the two would be informative. The image for September 13, 1981, is shown in Plate 1. (Plate 1 is shown here in black in white. The color version can be found in the separate color section in this issue.) High pigment concentrations near the coast, low concentrations offshore (lower left), and clouds offshore were characteristic of all images. Dates, sizes, and summary statistics for the subareas are given in Table 1. Subareas 7 and 10 were in coastal waters (high pigment concentrations) and 8 and 11 were in offshore waters (low pigment concentrations).

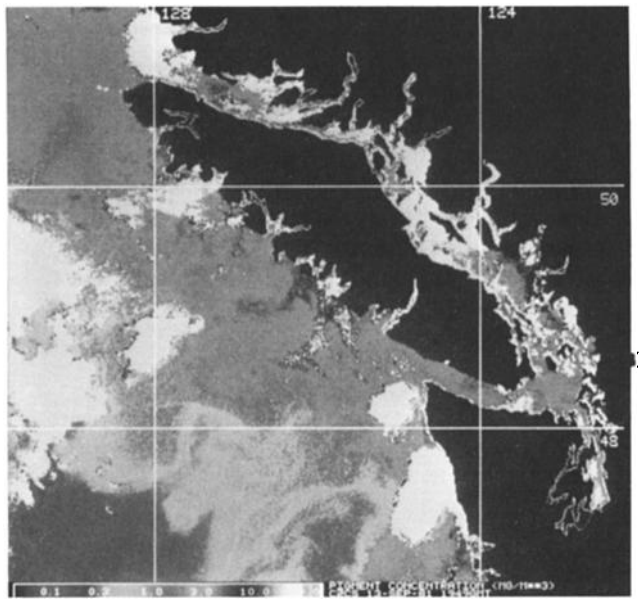

Plate 1. Estimated pigment concentration distribution for the CZCS image of September 13, 1981. (The color version and a complete description of this figure can be found in the separate color section in this issue.)

*Evaluation of the CZCS Pigment Algorithm*

Several investigators have compared satellite-derived pigment estimates with those from ship sampling [e.g., *Smith and Baker*, 1982; *Gordon et al.*, 1980, 1982, 1983*a*; *Abbott and Zion*, 1987]. Even when both modes of sampling are made on the same day, the ship data are not simultaneous with the satellite data (except possibly in one pixel), and the area coverage by ship cannot match that of a satellite. In July–August 1980 we carried out a 10-day cruise off Vancouver Island during which we sampled near-surface chlorophyll pigment from buckets and from the ship's seawater intake (~3 m) every hour while underway along the transect lines shown in Figure 2. The data, collected relatively evenly over the period July 30 to August 7, followed the frequency distribution, as a function of log (pigment), shown in Figure 3. The most frequent concentration occurred between 16 and 32 mg $m^{-3}$, an order of magnitude greater than in most of the cases where the algorithm has been tested previously. At such high pigment concentrations, the CZCS would receive backscattered irradiance from a very shallow depth layer: for a homogeneous ocean the depth $z_{90}$ of the layer from which 90% of the backscattered radiance emanates is approximately equal to the inverse of the diffuse attenuation coefficient [*Gordon and McCluney*, 1975]. From the formulae of *Austin and Petzold* [1981], $z_{90}$ for 490 nm is about 7 m for a pigment concentration of 1 mg $m^{-3}$ and about 0.6 m for 10 mg $m^{-3}$. To eliminate possible effects due to unmatched sampling depths between the CZCS and the ship intake, we have also shown (dashed line) in Figure 3 the pigment frequency distribution for only the bucket samples: the peak and shape of the distribution are unchanged. The frequency distribution (not shown) for bucket samples from only the evenly spaced parallel across-shelf transects (a more uniform spatial sampling pattern) also had the same peak and tail although it was based on many fewer samples.

The consistent frequency distribution for ship samples can be compared with frequency distributions from CZCS pigment concentrations within the polygon (marked by dashed lines) in Figure 2 for passes immediately preceding (July 28) and following (August 8) the period of ship sampling. These distributions, shown in Figure 4, are internally similar, but they differ markedly from the distribution of ship-based pigment concentrations. The CZCS images have a distribution with a tail toward higher pigment concentrations, but more importantly, their peak is near 3 mg $m^{-3}$, a factor of at least 5 less than for the ship samples. Mean chlorophyll concentrations for the two images are 4.6 and 3.6 mg $m^{-3}$, respectively, compared with a mean of 11.1 for all ship samples in Figure 3. We have also extracted 23 pixel values from the July 28 image to compare with ship samples taken inside the same pixels within 36 hours of the satellite pass. The regression line slope of chlorophyll pigment concentration upon CZCS-derived pigment concentration (both on linear scales) was 2.85 (with $r = 0.73$), consistent with the differences between the frequency distributions.

It is unlikely that the sampling area has been inadequately sampled by the CZCS because of clouds on July 28 (August 8): 95.4% (81.4%) of the pixels within the area encompassed by the dashed line were clear and included in the frequency distribution. Similarly, it is unlikely that the increased con-

TABLE 1. Summary Data for the Coastal Zone Color Scanner Images and Subareas Used in This Analysis

| | | | Mean | | | Standard Deviation | |
|---|---|---|---|---|---|---|---|
| Subarea | Size, pixels | Date | Pigment, mg $m^{-3}$ | Log Pigment, mg $m^{-3}$ | Log Pigment, bytes | Pigment, mg $m^{-3}$ | Log Pigment, bytes |
| 10 (coastal) | 100 × 100 | July 21, 1980 | 3.62 | 2.85 | 154.6 | 2.77 | 26.9 |
| | | July 26, 1980 | 2.94 | 2.38 | 148.0 | 2.94 | 20.7 |
| | | July 27, 1980 | 2.93 | 2.38 | 148.1 | 2.80 | 22.4 |
| | | July 28, 1980 | 3.11 | 2.72 | 153.0 | 2.20 | 17.6 |
| | | Aug. 8, 1980 | 2.35 | 2.24 | 145.8 | 0.88 | 10.5 |
| 7 (coastal) | 100 × 100 | Sept. 6, 1981 | 2.82 | 2.21 | 145.4 | 2.07 | 25.9 |
| | | Sept. 12, 1981 | 2.90 | 2.59 | 151.2 | 1.96 | 15.4 |
| | | Sept. 13, 1981 | 3.49 | 3.08 | 157.4 | 2.37 | 17.3 |
| 8 (offshore) | 100 × 100 | Sept. 6, 1981 | 0.54 | 0.48 | 89.8 | 0.27 | 18.1 |
| | | Sept. 12, 1981 | 0.82 | 0.65 | 101.3 | 0.73 | 24.2 |
| | | Sept. 13, 1981 | 0.67 | 0.60 | 98.0 | 0.34 | 18.0 |
| 11 (offshore) | 150 × 150 | Sept. 6, 1981 | 0.50 | 0.41 | 84.7 | 0.44 | 21.0 |
| | | Sept. 12, 1981 | 0.74 | 0.54 | 94.3 | 1.05 | 26.1 |
| | | Sept. 13, 1981 | 0.62 | 0.51 | 92.4 | 0.52 | 20.9 |

The log pigment columns represent statistics for the log-transformed values: byte value = $(\log_{10} \text{Chl} + 1.4)/0.012$.

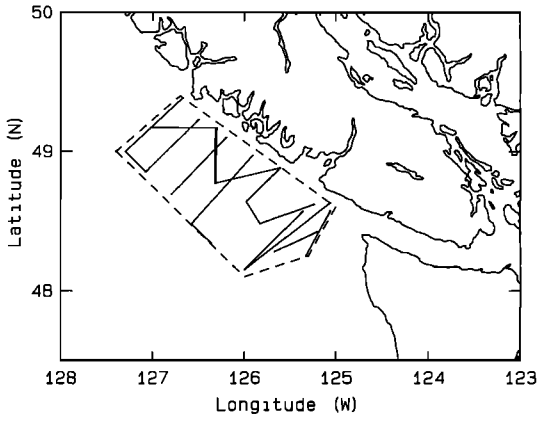


Fig. 2. A blowup of the area of Figure 1 showing the ship tracks (solid lines) along which were taken the near-surface chlorophyll samples with the frequency distribution shown in Figure 3. The area enclosed by the dashed line represents the CZCS pixels which were included in the frequency distributions shown in Figure 4.

centrations observed from the ship resulted from local growth: the high pigment concentrations were encountered on July 30, the first day of ship sampling, which would require the phytoplankton to have increased their biomass by nearly a factor of 10 in only 2 days, an unlikely but not impossible event. Also, a rather precipitous loss of pigment would have had to occur between the end of ship sampling and August 8, when the second CZCS image was acquired. Thus we believe that the pigment concentrations at the time of the two CZCS passes were substantially higher than the values derived from the imagery.

Two other characteristics of the CZCS pigment frequency distributions are evident in Figure 5. The bimodal distribution in the upper panel, formed from all clear pixels in the image of July 28, was characteristic of most clear images, which led to our earlier description of the subareas of Figure 1 as being "coastal" or "offshore". Because most of our sampling from ship has been over the continental shelf, we do not have a good historical data base of the pigment concentrations in local offshore waters. We do, however, commonly observe pigment concentrations as low as 0.1 mg $m^{-3}$, and in Figures 3

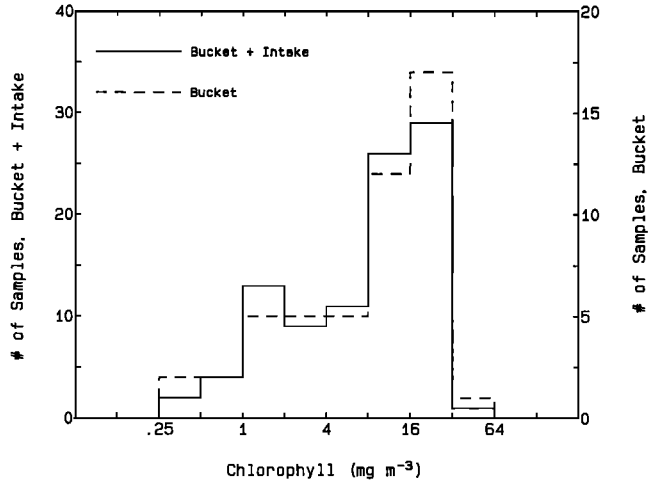


Fig. 3. Frequency distribution of surface phytoplankton chlorophyll pigment concentration obtained from ship sampling along the tracks shown in Figure 2 during the period July 30 to August 7, 1980. The dashed line represents bucket samples ($n = 49$), and the solid line represents bucket and ship intake (at about 3-m depth) samples ($n = 95$).

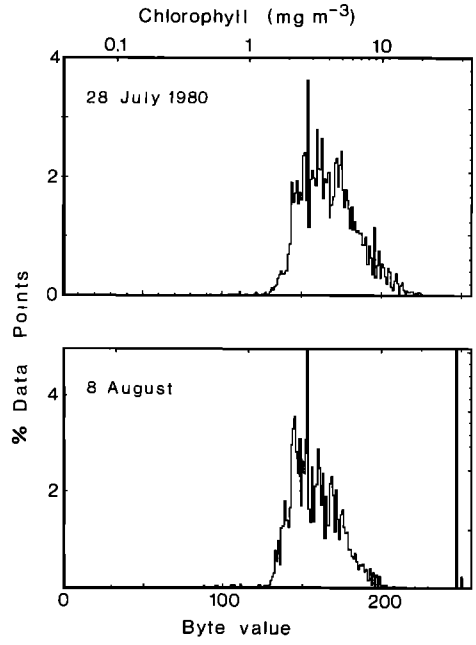


Fig. 4. Frequency distribution of surface pigment concentration estimated from the CZCS scanner for the area inside the dashed line in Figure 2, for (top) the July 28 image and (bottom) the August 8 image. The horizontal axis is log-transformed pigment with the lower scale in terms of the compressed format: byte value = ($\log_{10}$ Chl + 1.4)/0.012. High values near byte value 0 and near byte value 250 represent clouds and data beyond byte value 250.

and 4 there were proportionately more ship samples than CZCS values less than 1.0 mg $m^{-3}$. The discontinuity (marked by an arrow) in the distribution in the bottom panel of Figure 5, for subarea 10 on July 28, was frequently observed, especially in the subareas, and was in fact present (but less noticeable) in the whole image. It occurs at a pigment concentration of 1.5 mg $m^{-3}$, the test value in the pigment calculation algorithm for changing formulae when concentrations are sufficiently high that the upwelling radiance in the sensor channel centered on 443 nm is too small to be retrieved accurately because of increased absorbance by pigment. According to *Gordon et al.* [1983*a*], when the second formula yields a concentration of less than 1.5 mg $m^{-3}$, the initial value (greater than 1.5 mg $m^{-3}$) is retained, creating the possibility of an excess of values just greater than 1.5 mg $m^{-3}$.

Our data then indicate that the pigment concentrations deduced from the CZCS images off Vancouver Island are lower than those from ship samples by about a factor of 3. There are several possible reasons: the algorithms were developed for much lower pigment concentrations or for a different mix of accessory pigments than typically occur off Vancouver Island, few tests of the algorithms have been made at such high latitudes, the clear water calibrations for atmospheric absorbance effects may not work well if there is low radiance from aerosols over the whole scene, or there may have been a coccolithophore bloom causing high radiances not associated with pigments [e.g., *Holligan et al.*, 1983*b*]. Contrary to the results of Holligan et al., we found that during cruises at or near the same times of both our image sequences, coccolithophore species usually comprised about 10% of the total cell numbers and a much smaller percentage of the phytoplankton biomass, which was dominated by larger diatom cells [*Hill et al.*, 1982, 1983]. Hence it is highly unlikely that coccolithophores affected the radiances significantly.

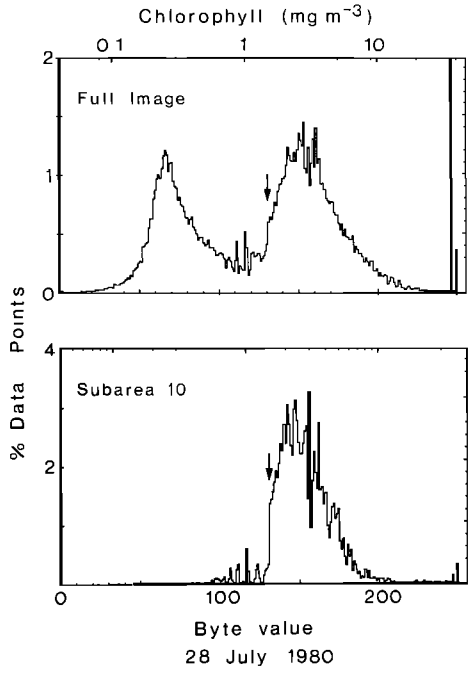


Fig. 5. Frequency distribution of surface pigment concentration estimated from the CZCS scanner as in Figure 4, for the whole image and for subarea 10. The arrows mark the pigment concentration 1.5 mg m$^{-3}$, where the algorithm to estimate pigment concentration changes.

As was discussed earlier, at pigment concentrations greater than 10 mg m$^{-3}$, the assumption that the water-leaving radiance at 670 nm was negligible is probably incorrect, and an iterative algorithm would be more appropriate if the necessary in-water optical measurements had been made. Nevertheless, we expect that the effects on spectrum calculations will be minimal. For autospectra we are interested mainly in the relative spectral distribution of variance, and we have found that the shape of the autospectrum is not highly sensitive to the shape of the frequency distribution; i.e. we found no significant difference between spectra of pigment and of log (pigment) values. For cross spectra, we are interested only in the degree of correlation between two images as a function of wave number, where pigment concentrations are normalized out automatically in the coherence function.

*Autospectra*

Calculation of the autospectrum is a necessary intermediate step in the calculation of the squared coherence spectrum. Recently, *Armi and Flament* [1985] cautioned against over interpretation of autospectra in relation to theories of turbulence. We recognize and share their concerns, but we have found the autospectrum to be a useful diagnostic tool. The one-dimensional spectra formed for the pigment images analyzed in this study tend to be smoothly varying and to obey a power law behavior (following a straight line on a log-log plot) over the range of wave numbers $\kappa$ (actually inverse wavelengths) from 0.03 to 0.3 km$^{-1}$. In the offshore waters (Figure 6), the slope is uniformly near $\kappa^{-2}$; in the nearshore "coastal" waters the slope varies from $\kappa^{-1.5}$ to $\kappa^{-2}$, consistent with the hypothesis that there is more energy input at shorter length scales near the coast, from tidal mixing, interaction with bathymetry, and more rapid growth of phytoplankton and because of a shorter internal Rossby radius of deformation. We note that to preserve variance we have summed azimuthally in wave number space, rather than averaging azimuthally. Because the area of concentric rings of constant width $\Delta\kappa$ increases proportionally to $\kappa$, our spectra are less steep than those formed from azimuthal averages by a factor of $\kappa^{+1}$.

*Cross-Spectra and Squared Coherence*

In Figure 7 we present spectra of squared coherence for the three pair combinations of images for subarea 11, the largest and hence the one with spectral estimates at the largest scales. For $\kappa$ of less than 0.07 km$^{-1}$ (i.e., for wavelengths longer than about 15 km), the squared coherence is clearly higher than the 90% level for the pair of images 1 day apart. For the pair of images 6 days apart, all correlation has been lost for $\kappa$ greater than 0.02 km$^{-1}$. For the pair of images 7 days apart, all correlation has been lost for $\kappa$ greater than 0.01 km$^{-1}$. The 90% significance level decreases with increasing $\kappa$ because, as before, the number of spectral estimates within concentric rings of constant $\Delta\kappa$ increases proportionally to $\kappa$.

To summarize the data from all pairs of images, we need to form the squared cross-correlation function between images, $r_{12}{}^2(0, \tau)$. Because the correlation coefficient in geophysical data tends to be dominated by the largest scales, in this case by trends over the scale of the subarea, we also form the spectral analog to $r^2$, the squared coherence $K_{12}{}^2(\kappa)$. In this notation the arguments 0 and $\tau$ signify that the cross correlation is formed between images at spatial lag 0 but at time lag $\tau$, and the argument $\kappa$ indicates that there is a squared

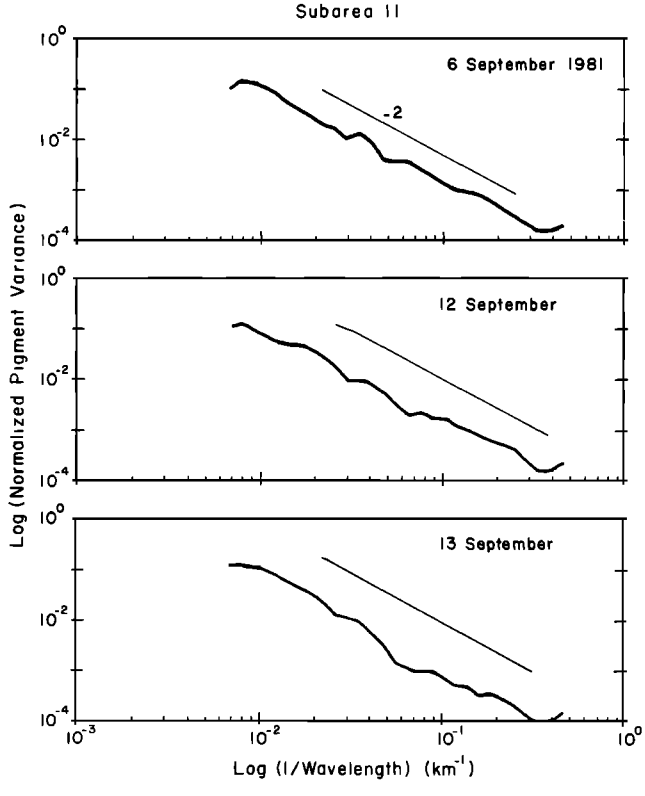


Fig. 6. Autospectra for the three images of subarea 11 on a log-log plot. The azimuthal summations of spectral variance were performed over 32 bands with geometrically increasing bandwidth $\Delta\kappa$, which are of constant width on this logarithmic representation. Only the estimates for wavelengths less than or equal to the subarea dimension are plotted. Straight lines with a $\kappa^{-2}$ slope characteristic of power law behavior have been drawn for reference.

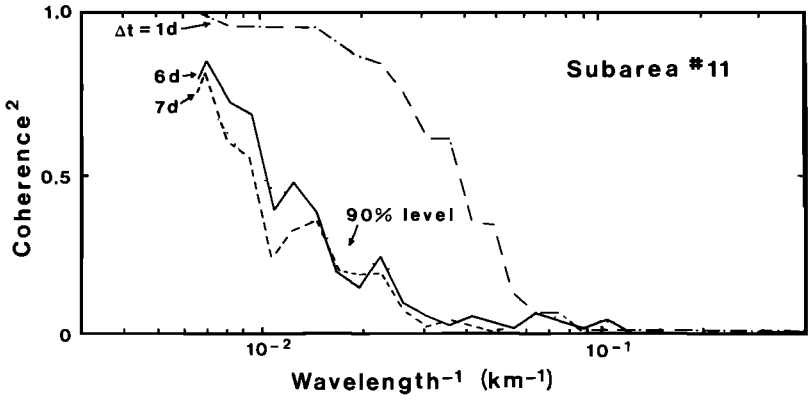


Fig. 7. Squared coherence spectra for pairs of the three images of September 1981. As in Figure 6, the spectral estimates are for wave bands of constant logarithmic width. The 90% levels for coherence significantly greater than those expected between two random uncorrelated fields were obtained by taking the tenth highest estimate (in each wave band) out of 99 realizations of coherence spectra calculated between synthetic random uncorrelated fields with a specified $\kappa^{-1.5}$ power law behavior.

coherence estimate for each wave band centered on $\kappa$ (the $\tau$ time separation is assumed).

We have plotted in Figure 8*a* (top panel) the cross correlation coefficient $r$ (rather than $r^2$, to preserve a larger range of values) for all pairs of subarea images analyzed. The values from each sequence are joined by a line, and coastal or offshore sequences are identified. The degree of correlation in offshore subareas is higher than for coastal areas at all time separations out to 7 days. For all three subareas (7, 8, and 11), the September 1981 series shows a monotonic loss of correlation with increasing time separation. The July–August 1980 series (subarea 10) shows correlation after 1 week similar to

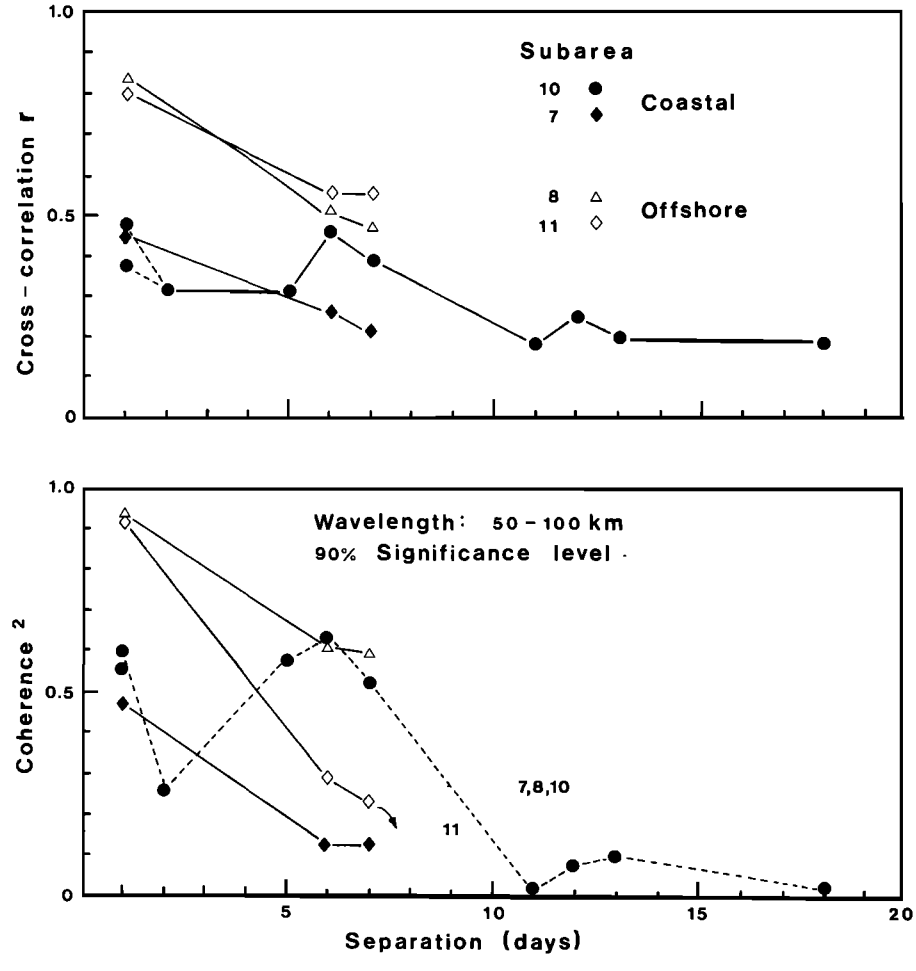


Fig. 8*a*. (Top) Cross correlation $r(0, \tau)$ at 0 spatial lag, for all pairs of images plotted against the time separation between image pairs $\tau$. (Bottom) Squared coherence between pairs of images for the wavelength band 50–100 km also plotted against time separation. The 90% significance levels are as in Figure 7 except that those for subareas 7, 8, and 10 (100 km square) were determined from 999 realizations. Subarea 10 is from 1980; the others are from 1981.

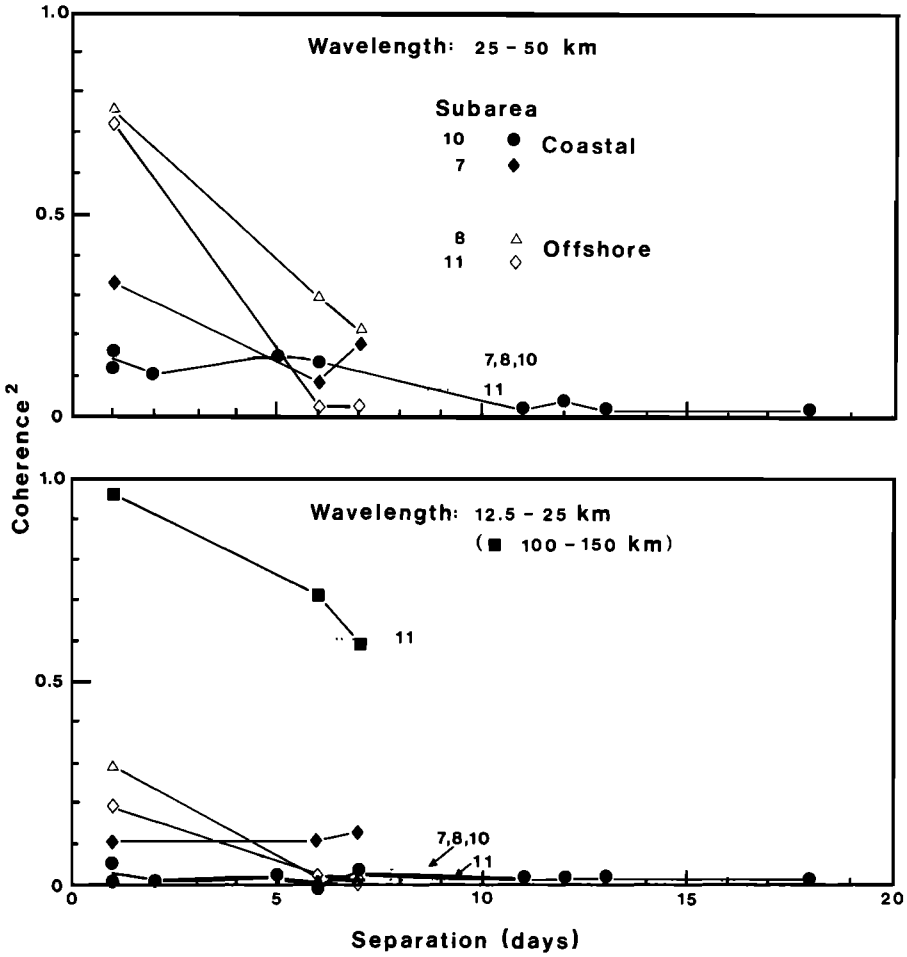


Fig. 8*b*. Squared coherence for the wavelength bands (top) 25–50 km and (bottom) 12.5–25 km and 100–150 km (subarea 11 only).

that after 1 day, with lower correlations at separations of 2 and 5 days. This series includes time separations out to 18 days, but the loss of correlation was apparently complete after 11 days.

To present the squared coherence spectra in an analogous form, we summed the spectral estimates into several broad wave number bands and plotted the resulting estimates against time separation for each wave number band. We have plotted in the bottom panel of Figure 8*a* the results for the largest-scale wave band common to all subareas, wavelengths of 50–100 km (or $\kappa$ of 0.01–0.02 km$^{-1}$). The trends for all sequences are similar to those for the cross-correlation coefficient: the 1981 series all lose coherence monotonically while the 1980 series (one subarea) retains coherence out to a time separation of 1 week, except for a low coherence at a $\tau$ of 2 days. We also note that subarea 11 loses coherence more rapidly than subarea 8 (which is embedded within subarea 11) although the coherence in both subareas is still above the 90% significance level after 7 days.

The same sequences have been plotted against time separation in Figure 8*b* for the wavelength bands 25–50 km ($\kappa$ = 0.02–0.04 km$^{-1}$), 12.5–25 km ($\kappa$ = 0.04–0.08 km$^{-1}$), and (for subarea 11 only) 100–150 km ($\kappa$ = 0.01–0.007 km$^{-1}$). For the band 25–50 km, only the offshore subarea 8 retains significant coherence after 1 week, subareas 7 and 11 seem to have lost any coherence after 5 days, and the coherence of the coastal subarea 10 remained near the 90% significance level out to a $\tau$ of 6 days but was clearly below that level after 11 days. For the band 12.5–25 km, only the offshore subareas 8 and 11 were clearly coherent for a $\tau$ of 1 day, but the coherence had dropped below the significance level after 6 days. The coastal subarea 7 retained a constant "significant" coherence at all time separations, probably due to a common ($x$, $y$) trend. We had tested several images at random for removal of an ($x$, $y$) plane, but the fitted planes were not significant, so we did not include that step in the data analysis. For the largest band, 100–150 km, the coherences of subarea 11 were higher than any other coherences, consistent with the intuitive idea that larger-scale patterns should retain their identity longer, but the 90% significance level was also the highest because estimates from that band were drawn from the smallest number of spectral estimates.

## Discussion

For two sequences of CZCS satellite color images, we have calculated two-dimensional autospectra and cross spectra and have summed the spectra azimuthally to obtain equivalent one-dimensional spectra. The autospectra, a necessary step in the calculation of cross spectra, display a power law behavior of $\kappa^{-1.5}$ to $\kappa^{-2}$, with exponents near $-2$ predominant. These results are consistent with earlier findings for ocean color of *Gower et al.* [1980], whose band-averaged spectra with exponents near $-3$ are equivalent to the $-2$ exponents for band-integrated spectra obtained in this study; and with find-

ings for sea surface temperature of *Deschamps et al.* [1981], who inferred spectral power law exponents of −1.5 to −2.3 from structure function calculations. While we acknowledge the cautionary remarks of *Armi and Flament* [1985] regarding the interpretation of spectrum shapes in terms of turbulence theories, we note that *Holloway* [1986] obtained spectral power law exponents of between −1 and −2 in models of phytoplankton growing in two-dimensional turbulent flow from both numerical simulations and closure theory.

From the rates of falloff of squared coherence with increasing time separation, we have estimated for the study area off the west coast of Canada the time rate of decorrelation of sea surface pigment patterns at different length scales. At length scales greater than 50 km, offshore patterns were still coherent after 1 week. Extrapolation suggests that coherence would fall below the 90% significance level after 8–10 days. At length scales in the range 25–50 km, the offshore patterns remained marginally coherent after 1 week, but the coastal patterns lost any coherence after 2–5 days. At length scales in the range 12.5–25 km, offshore patterns 1 day apart were coherent, but coastal patterns were only marginally so. All correlation in this band had disappeared by 5–7 days. An extension of the model of *Holloway* [1986] to a continental slope region with variable bottom topography results in the lagged correlation coefficient for simulated plankton biomass patterns decreasing with increasing time separation, then flattening out after 3–4 days in the case of an alongshore current and after 10–12 days in the case of no mean current [*Eert et al.*, 1987]. The simulation area was several hundred kilometers on a side.

The findings presented here are consistent with those of other studies (referred to in the introduction) from eastern boundary current regions [*Kelly*, 1983, 1985; *Denman and Freeland*, 1985; *Kosro*, 1987]. The decorrelation times are somewhat shorter than the time inferred by *Denman and Freeland* [1985]. They estimated a decorrelation time scale of 10 days for horizontal ocean currents, from a broad spectral peak centered on a frequency equivalent to a 20-day period (for a 3-year (1979–1981) current record from a meter moored at 100 m at 48°15'N, 125°48'W within the study area shown in Figure 1). One would expect near-surface patterns to be more variable because of surface forcing and inputs, and also one would expect phytoplankton biomass (because it is being created and destroyed or removed from the surface layer) to vary more with time than do physical variables such as currents or geopotential height. Although the wind forcing off Vancouver Island in summer is a relative minimum (wind speed cubed is less than 300 $m^3 s^{-3}$ compared with more than 1300 $m^3 s^{-3}$ off the northern California CODE study area [*Husby and Nelson*, 1982]), tidal-forced diurnal shelf waves [*Crawford*, 1984; *Crawford and Thomson*, 1984], a topographic upwelling gyre [*Freeland and Denman*, 1982; *Denman and Freeland*, 1985; *Freeland*, 1988], and offshore baroclinic eddy activity [*Ikeda et al.*, 1984; *Thomson*, 1984] all provide sources of variability on scales of days to weeks that create and destroy near-surface pigment patterns.

The result that patterns at the mesoscale (of the order of 60–100 km) lose coherence after 10 days seems at first to be suspect in light of recent observations of persistent eddies and upwelling filaments. However, this analysis is Eulerian, and translational motion alone will result in decorrelation: a 10 cm $s^{-1}$ current will advect a 60-km-diameter eddy half its diameter in just over 3 days (resulting in a zero crossing of the temporal correlation function $r(\tau)$ in this simplified example). To remove translational and rotational motion, two-dimensional Lagrangian techniques involving spatially lagged correlation are available; they are presently used to determine ice or water motion between pairs of images [*Ninnis et al.*, 1986; *Emery et al.*, 1986]. Current patterns [*Joyce and Kennelly*, 1985] and pigment biomass patterns [*Smith and Baker*, 1985] associated with coherent persistent structures such as warm-core rings can be readily mapped and followed for months even from ship, although their Eulerian decorrelation time would be of the order of weeks at most.

Phytoplankton are also a nonconservative scalar tracer generating variance at mesoscale wavelengths on time scales from a few days to a few months [e.g., *Bennett and Denman*, 1985]. In the near future we plan to compare decorrelation rates for temperature and pigments in the same area over the same time period and to calculate cross spectra between thermal and pigment images in an effort to determine from two-dimensional, highly resolved data if biological processes alone create significant pattern.

The most obvious next step, however, is to extend this analysis to a larger number of image sequences and to other representative geographical regions, especially to aid the Global Ocean Flux Study (GOFS) program in determining appropriate averaging for the estimation of primary production over the highly productive, but highly variable, oceanic margins (spatial) and spring bloom periods (temporal). It is already clear from this work that 1-month composite scenes will not preserve mesoscale patterns along the continental margins and that local production and eddy transport of biogenic materials in these regions will need to be evaluated on shorter scales from some combination of remote imagery and in situ sampling.

*Acknowledgments.* We thank A. Dolling of Interact Research and Development and P. Zion of the Jet Propulsion Laboratory for their help in the analysis of these data, G. Holloway and D. Ramsden for helpful discussions, and R. Brown, D. Glover, H. Freeland, W. Hsieh, and an anonymous reviewer for their comments on various drafts. The Scripps Satellite Oceanography Facility is supported by the National Science Foundation, the Office of Naval Research, and the National Aeronautics and Space Administration (NASA). This research was supported by NASA (to JPL) and by the Canadian Department of Fisheries and Oceans.

## REFERENCES

Abbott, M. R., and P. M. Zion, Spatial and temporal variability of phytoplankton pigment off northern California during Coastal Ocean Dynamics Experiment 1, *J. Geophys. Res.*, *92*, 1745–1755, 1987.

Armi, L., and P. Flament, Cautionary remarks on the spectral interpretation of turbulent flows, *J. Geophys. Res.*, *90*, 11,779–11,782, 1985.

Austin, R. W., and T. J. Petzold, The determination of the diffuse attenuation coefficient of sea water using the Coastal Zone Color Scanner, in *Oceanography from Space*, edited by J. F. R. Gower, pp. 239–256, Plenum, New York, 1981.

Bennett, A. F., and K. L. Denman, Phytoplankton patchiness: Inferences from particle statistics, *J. Mar. Res.*, *43*, 307–335, 1985.

Brewer, P. G., K. W. Bruland, R. W. Eppley, and J. J. McCarthy, The Global Ocean Flux Study (GOFS): Status of the U.S. GOFS program, *Eos Trans. AGU*, *67*, 827–832, 1986.

Brown, O. B., and R. E. Cheney, Advances in satellite oceanography, *Rev. Geophys.*, *21*, 1216–1230, 1983.

Crawford, W. R., Energy flux and generation of diurnal shelf waves along Vancouver Island, *J. Phys. Oceanogr.*, *14*, 1600–1607, 1984.

Crawford, W. R., and R. E. Thomson, Diurnal-period continental shelf waves along Vancouver Island: A comparison of observations with theoretical models, *J. Phys. Oceanogr.*, *14*, 1629–1646, 1984.

Denman, K. L., and H. J. Freeland, Correlation scales, objective mapping and a statistical test of geostrophy over the continental shelf, *J. Mar. Res.*, *43*, 517–539, 1985.

Denman, K. L., and T. M. Powell, Effects of physical processes on planktonic ecosystems in the coastal ocean, *Oceanogr. Mar. Biol. Annu. Rev.*, *22*, 125–168, 1984.

Deschamps, P. Y., R. Frouin, and L. Wald, Satellite determination of the mesoscale variability of the sea surface temperature, *J. Phys. Oceanogr.*, *11*, 864–870, 1981.

Eert, J., G. Holloway, J. F. R. Gower, K. Denman, and M. Abbott, Inference of physical/biological dynamics from synthetic ocean colour images, *Adv. Space Res.*, *7*(2), 89–93, 1987.

Emery, W. J., A. C. Thomas, M. J. Collins, W. R. Crawford, and D. L. Mackas, An objective method for computing advective surface velocities from sequential infrared satellite images, *J. Geophys. Res.*, *91*, 12,865–12,878, 1986.

Esaias, W. E., G. C. Feldman, C. R. McClain, and J. A. Elrod, Monthly satellite-derived pigment distribution for the North Atlantic Ocean basin, *Eos Trans. AGU*, *67*, 835–837, 1986.

Freeland, H. J., Lagrangian statistics on the Vancouver Island continental shelf, *Atmos. Ocean*, *26*, 267–281, 1988.

Freeland, H. J., and K. L. Denman, A topographically controlled upwelling center off southern Vancouver Island, *J. Mar. Res.*, *40*, 1069–1093, 1982.

Gordon, H. R., and W. R. McCluney, Estimation of the depth of sunlight penetration in the sea for remote sensing, *Appl. Opt.*, *14*, 413–416, 1975.

Gordon, H. R., D. K. Clark, J. L. Mueller, and W. A. Hovis, Phytoplankton pigments from the Nimbus-7 Coastal Zone Color Scanner: Comparisons with surface measurements, *Science*, *210*, 63–66, 1980.

Gordon, H. R., D. K. Clark, J. W. Brown, O. B. Brown, and R. H. Evans, Satellite measurement of the phytoplankton pigment concentration in the surface waters of a Gulf Stream ring, *J. Mar. Res.*, *40*, 491–502, 1982.

Gordon, H. R., D. K. Clark, J. W. Brown, O. B. Brown, R. H. Evans, and W. W. Broenkow, Phytoplankton pigment concentrations in the Middle Atlantic Bight: Comparison of ship determinations and CZCS estimates, *Appl. Opt.*, *22*, 20–36, 1983*a*.

Gordon, H. R., J. W. Brown, O. B. Brown, R. H. Evans, and D. K. Clark, Nimbus 7 CZCS: Reduction of its radiometric sensitivity with time, *Appl. Opt.*, *22*, 3929–3931, 1983*b*.

Gower, J. F. R., K. L. Denman, and R. J. Holyer, Phytoplankton patchiness indicates the fluctuation spectrum of mesoscale oceanic structure, *Nature*, *288*, 157–159, 1980.

Haury, L. R., J. A. McGowan, and P. H. Wiebe, Patterns and processes in the time-space scales of plankton distributions, in *Spatial Pattern in Plankton Communities*, edited by J. H. Steele, pp. 277–327, Plenum, New York, 1978.

Hill, S., K. Denman, D. Mackas, and H. Sefton, Ocean ecology data report: Coastal waters off southwest Vancouver Island spring and summer 1980, *Can. Data Rep. Hydrogr. Ocean Sci.*, *4*, 103 pp., 1982.

Hill, S., K. Denman, D. Mackas, H. Sefton, and R. Forbes, Ocean ecology data report: Coastal waters off southwest Vancouver Island spring and summer 1981, *Can. Data Rep. Hydrogr. Ocean Sci.*, *8*, 93 pp., 1983.

Holligan, P. M., M. Viollier, C. Dupouy, and J. Aiken, Satellite studies on the distributions of chlorophyll and dinoflagellate blooms in the western English Channel, *Cont. Shelf Res.*, *2*, 81–96, 1983*a*.

Holligan, P. M., M. Viollier, D. S. Harbour, P. Camus, and M. Champagne-Philippe, Satellite and ship studies of coccolithophore production along a continental shelf edge, *Nature*, *304*, 339–342, 1983*b*.

Holloway, G., Eddies, waves, circulation, and mixing: Statistical geofluid mechanics, *Annu. Rev. Fluid Mech.*, *18*, 91–147, 1986.

Husby, D. M., and C. S. Nelson, Turbulence and vertical stability in the California Current, *Rep. 23*, pp. 113–129, Calif. Coop. Oceanic Fish. Invest., La Jolla, 1982.

Ikeda, M., L. A. Mysak, and W. J. Emery, Observation and modeling of satellite-sensed meanders and eddies off Vancouver Island, *J. Phys. Oceanogr.*, *14*, 3–21, 1984.

Joyce, T. M., and M. A. Kennelly, Upper-ocean velocity structure of Gulf Stream warm-core ring 82B, *J. Geophys. Res.*, *90*, 8839–8844, 1985.

Kelly, K. A., Swirls and plumes or application of statistical methods to satellite-derived sea surface temperatures, Ph. D. thesis, *Ref. 83-15*, 210 pp., Scripps Inst. of Oceanogr., Univ. of California, San Diego, Aug. 1983.

Kelly, K. A., The influence of winds and topography on the sea surface temperature patterns over the northern California slope, *J. Geophys. Res.*, *90*, 11,783–11,798, 1985.

Kosro, P. M., Structure of the coastal current field off northern California during the Coastal Ocean Dynamics Experiment, *J. Geophys. Res.*, *92*, 1637–1654, 1987.

Maul, G. A., *Introduction to Satellite Oceanography*, 606 pp., Nijhoff, Dordrecht, Netherlands, 1985.

National Academy of Sciences, *Global Ocean Flux Study: Proceedings of a Workshop*, National Academy Press, Washington, D. C., 1984.

Ninnis, R. M., W. J. Emery, and M. J. Collins, Automated extraction of pack ice motion from advanced very high resolution radiometer imagery, *J. Geophys. Res.*, *91*, 10,725–10,734, 1986.

Njoku, E. G., T. P. Barnett, R. M. Laurs, and A. C. Vastano, Advances in satellite sea surface temperature measurement and oceanographic applications, *J. Geophys. Res.*, *90*, 11,573–11,586, 1985.

Robinson, I. S., *Satellite Oceanography: An Introduction for Oceanographers and Remote-Sensing Scientists*, 455 pp., Ellis Horwood, Chichester, England, 1985.

Smith, R. C., and K. S. Baker, Oceanic chlorophyll concentrations as determined by satellite (Nimbus-7 coastal zone color scanner), *Mar. Biol.*, *66*, 269–279, 1982.

Smith, R. C., and K. S. Baker, Spatial and temporal patterns in pigment biomass in Gulf Stream warm-core ring 82B and its environs, *J. Geophys. Res.*, *90*, 8859–8870, 1985.

Smith, R. C., and W. H. Wilson, Ship and satellite bio-optical research in the California Bight, in *Oceanography From Space*, edited by J. F. R. Gower, pp. 281–294, Plenum, New York, 1981.

Steele, J. H. (Ed.), *Spatial Pattern in Plankton Communities*, 470 pp., Plenum, New York, 1978.

Stewart, R. H., *Methods of Satellite Oceanography*, 360 pp., University of California Press, Berkeley, 1985.

Stommel, H., Varieties of oceanographic experience, *Science*, *139*, 572–576, 1963.

Thomson, R. E., A cyclonic eddy over the continental margin of Vancouver Island: Evidence for dynamical instability, *J. Phys. Oceanogr.*, *14*, 1326–1348, 1984.

Zion, P. M., Description of algorithms for processing coastal zone color scanner (CZCS) data, *Publ. 83-98*, 29 pp., Jet Propul. Lab., Pasadena, Calif., 1983.

M. R. Abbott, College of Oceanography, Oregon State University, Oceanography Administration Building 104, Corvallis, OR 97331.

K. L. Denman, Institute of Ocean Sciences, P.O. Box 6000, Sidney, B. C., Canada, V8L 4B2.

(Received September 23, 1987;
accepted December 8, 1987.)

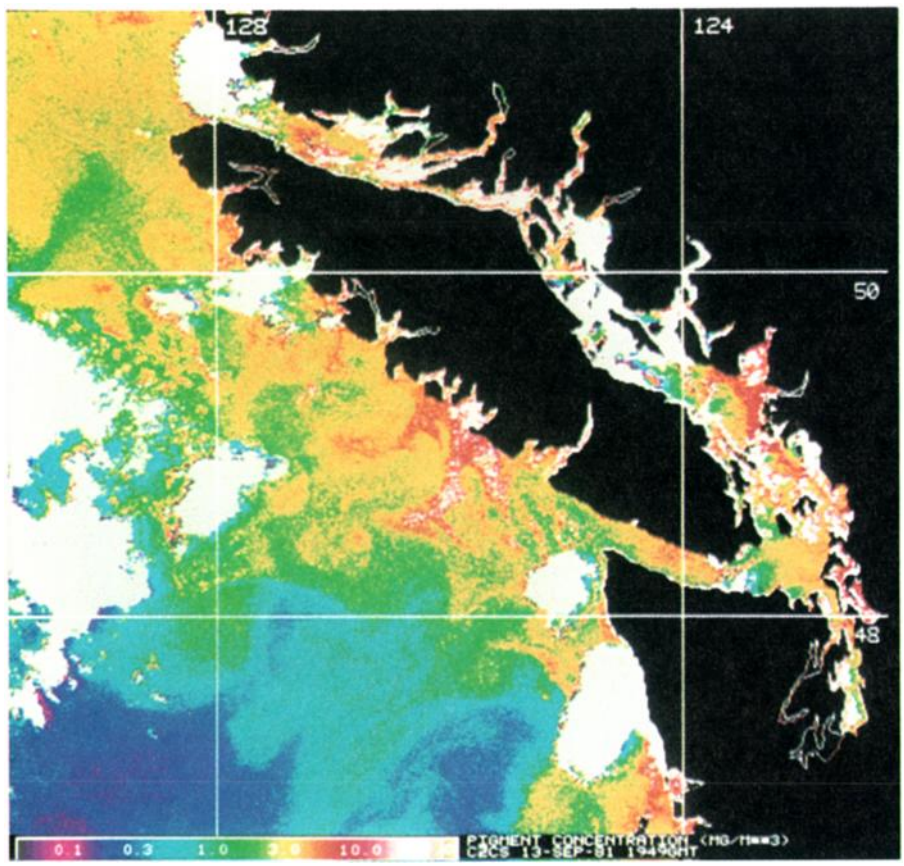


Plate 1 [*Denman and Abbott*]. Estimated pigment concentration distribution for the CZCS image of September 13, 1981. The color scale, ranging from 0.3 to 30 mg $m^{-3}$, is shown at the bottom.